Categorization of iso-pentane flashing spray based on morphology, thermodynamical and mechanical effects

Xiang-Wei Lin, Dong-Qing Zhu, Zhi-Fu Zhou, Shu-Qin Xue, Teng-Fei Liu, Jia-Feng Wang, Bin Chen, Eric Lichtfouse

International Journal of Multiphase Flow 170 (2024) 104657

https://doi.org/10.1016/j.ijmultiphaseflow.2023.104657

Categorization of iso-pentane flashing spray based on morphology, thermodynamical and mechanical effects

Xiang-Wei Lin [a], Dong-Qing Zhu [a], Zhi-Fu Zhou [a,*], Shu-Qin Xue [a], Teng-Fei Liu [a], Jia-Feng Wang [a], Bin Chen [a], Eric Lichtfouse [a,b]

[a] State Key Laboratory of Multiphase Flow in Power Engineering, Xi'an Jiaotong University, Xi'an 710049, China
[b] Aix-Marseille Univ, CNRS, IRD, INRA, CEREGE, Aix-en-Provence 13100, France

Keywords:
Flashing spray characteristics
Superheated iso-pentane
Thermodynamic nonequilibrium effect
Mechanical effect
Quantitative criterion
Hazardous release

A B S T R A C T

Accidental release of superheated liquids is typically accompanied with hazardous flashing jets. Indeed, flashing jets undergo fragmentation into massive fine droplets, thus forming ideal circumstances for fires and explosion. To gain a deeper understanding of depressurized release, we studied the dynamics of iso-pentane at superheats of 40–80 °C and injection pressures of 0.6–3.0 MPa. The internal flow pattern and external spray morphology are visualized at quasi-steady stage using a high-speed camera. Results show that the flashing patterns can be classified into non-flashing, transitional flashing, and flare flashing arising from the interaction between thermodynamic and mechanical effects. The contribution of thermodynamic effect decreases as mechanical effect intensifies, due to the suppression of bubble nucleation and burst. We propose the index k, based on $JaR_p = k(We_v Oh)^{-1/7}$, to identify different flashing regions, i.e., k below 211 for non-flashing, k between 212 and 425 for transitional flashing, and k above 425 for flare flashing. Besides, the microscopic characteristics involving droplet velocity and diameter distribution are investigated and a new correlation for drop size is proposed, which is dependent on factors such as nozzle aspect ratio, mechanical force, and thermodynamic force. These findings should help to define policies to decrease the risk associate with flashing jets.

1. Introduction

Many flammable, poisonous, and explosive liquids are often stored under high-pressure conditions in the industry (Zhu et al., 2019). Superheated liquids are characterized by temperature that exceed their boiling point at atmospheric pressure, which induces a metastable state (Zhu et al., 2020). As a consequence, the occurrence of slight accidental leakage on the surface of tank or pipe results in a rapid two-phase change, thereby expelling a tremendous amount of energy into the environment (Tang et al., 2022). This phase change usually leads to the formation of flashing jets (Mansour and Müller, 2019). In contrast to single-phase emission of liquid or gas, the phase-changing flashing jet would breakup into abundant fine droplets due to the synergistic effect of thermodynamic nonequilibrium and mechanical action. Afterwards, a significant quantity of atomized droplets and evaporated gas disperse and suspend within the air environment of the site's accident, thus creating favorable conditions for fires and explosions (Guo et al., 2019b; Wang et al., 2023b; Wu et al., 2022). The potential consequences of such accidents pose a severe threat to human life, economy, and environment (Polanco et al., 2010), yet flashing mechanisms are poorly known. Therefore, it is important to elucidate the formation pattern and flow behavior of two-phase change during the release of superheated liquids.

In particular, during the accidental emission of superheated liquids, one basic challenge is to identify the spatial distribution and dynamic characteristics of droplets (Loureiro et al., 2021). In general, several spray atomization behaviors, i.e., turbulence, bubble growth, slug, and annular flow, coexist during the flash-boiling process (Ji et al., 2023). Moreover, obtaining detailed information regarding droplets diameter and distribution would help to assess the potential zone that might experience burn or crack. Consequently, researchers have conducted experiments wherein the flashing spray is formed to simulate the accidental leakage (Allen, 1998, 1988). The optical imaging technique allows for the observation of several morphological characteristics of the flashing spray, i.e., cone angle, penetration length, and width (Guo et al., 2019a; Li et al., 2019; Zhifu et al., 2012). For instance, Zhou et al. (2021b) found that the morphology of R404A flashing spray followed a dynamic evolution prior to reaching a bowl-shape structure in the steady

* Corresponding author.
E-mail address: zfzhou@mail.xjtu.edu.cn (Z.-F. Zhou).

Nomenclature

c_p	heat capacity (J kg^{-1} K^{-1})
C_d	discharge coefficient
d_0	nozzle diameter (m)
D	spray width (m)
D_{32}	Sauter mean diameter (m)
E	bubble burst energy (J)
ΔG	Gibbs free energy (J mol^{-1})
h_{fg}	enthalpy (J kg^{-1})
J	nucleation rate (m^{-3})
k	index
k_b	Boltzmann constant
L	specified distance (m)
P	pressure (Pa)
T	temperature (°C)
u	velocity (m s^{-1})

Subscripts

0	ambient
in	inlet
inj	injection
l	liquid phase
v	vapor phase
s	saturation
th	theory

Greek symbols

θ	spray cone angle (°)
λ	thermal conductivity (W m^{-1} K^{-1})
μ	viscosity (Pa s)
ρ	density (kg m^{-3})
σ	surface tension (N m^{-1})
ϕ	spray diameter (m)
χ	energy barrier
ω	instability growth rate (m s^{-1})
φ	correction factor

Acronyms

Ja	Jacob number
Oh	Ohnesorge number
Re	Reynold number
R_p	superheat degree
We	Weber number

state. The droplet properties, such as microscopic diameter, velocity, and temperature, can be further analyzed using a particle dynamic analyzer (Jing et al., 2017; Wu et al., 2021; Zhou et al., 2017).

Nevertheless, the completion of flashing atomization cannot be easily acquired, due to various influencing factors, including fluid dynamics and heat and mass transfer. For thermal nonequilibrium-induced flashing, the superheated spray features bubble nucleation, growth, and burst (Zhou et al., 2021a). When the temperature is low, evaporation of surface droplets starts first, whereas boiling under superheat commences with a breakup of the liquid core (Lamanna et al., 2014). Among which, the bubble burst directly affects the spray pattern, which is known as thermodynamic breakup. Since the 1960s, Brown and York (1962) analyzed the spray patterns and droplet kinetics of water and Freon-11, and found that superheat is the prerequisite for producing flash-atomization. Following this pioneering experiment, many scholars have conducted research on the phenomenon of flashing spray. Günther and Wirth (2013) examined the impact of superheat on the internal bubble evolution and the external spray morphology. Their finding revealed that when the superheat raised to 30 °C, a discernible nucleation appeared within the nozzle capillary, accompanied with a pronounced disintegration of spray jet. Zhang et al. (2015) also found that both bubble formation inside the nozzle and methanol jet breakup near the nozzle exit were strongly affected by the superheat. They suggested that the area fraction of liquid jet has positive influence on bubble number density, indicating the breakup of superheated liquid is directly linked to the strength of bubble formation. As well, Moulai et al. (2015) found that flash boiling contributed to generate wide plume angles, while non-flashing caused narrow plume angle that diminished the plume-to-plume interaction. According to Luo and Haidn (2016), an increase in superheat led to a progressive transformation in the spray pattern of the cryogenic fluid. The transition occurred from mechanical atomization to fully flashing, characterized by a substantial bell-shaped angle. Recently, Soo Yu et al. (2023) compared the spray characteristics of n-heptane and liquefied petroleum gas fuel across different flashing situations. Results showed that the increase in superheat expanded the spray plume of both types of fuel in the central axial direction.

The superheated liquid released in the environment through the nozzle exhibits distinctive drop sizes when subjected to sudden depressurization. Under high injection pressure, the liquid jet breaks up into finer droplets due to the amplification of turbulent disturbances (Hwang et al., 2020; Sher et al., 2008). Besides, the breakup mechanism of liquid jet is also associated with the combination of viscous force that exhibits a stabilizing effect by withstanding change in jet geometry, inertial force that is reflected in jet velocity, and aerodynamic force that shows the interaction between jet and air. These forces collectively contribute to the mechanical breakup of liquid jet, which is described as mechanical effect. Hervieu and Veneau (1996) showed that the drop size decreased and velocity increased at higher spray pressure. The similar trends were observed by Witlox et al., (2017a, 2010, 2017b), who measured the drop size in the far-field region, at spray distance more than 40 cm for spray dispersion under different pressures. Taking R134a as a release medium, Yildiz et al. (2004) investigated the characteristics of two-phase flashing jet under a harsh environment, and found that the spray pressure had a strong influence on the onset breakup location and particle mean velocity, but less on the particle diameter. For the flashing spray of iso-octane, Wang et al. (2016) found that higher pressure induced an early expansion of cone angle, then a smaller cone angle at quasi-steady stage, owing to the dominance of hydraulic force. In order to clearly reflect the impact of internal flow on external spray morphology, Wang et al. (2017) proposed a transparent tube nozzle for observing the flow pattern of R134a. Due to the primary breakup near the nozzle, higher void fraction inside the nozzle was positively related to the formation of fine droplets. Besides, the growth of spray cone angle presented an exponential correlation with the injection pressure.

Overall, most recent research has provided deep insights pertaining to the downstream flashing behaviors and droplet dynamics that occur after a sudden release. With it, however, the majority of efforts has primarily been concentrated on the quasi-steady atomization characteristics in the far-field region, while limited attention on the non-steady primary breakup of superheated liquids in the near-field region. For this purpose, flashing spray experiments containing internal flow and external spray are performed in this work. Then, the formation of flashing spray is governed by the synergic action of thermodynamic and mechanical forces. As a result, superheat and pressure are regarded as the essential source conditions during the accidental emission process. Although researchers suggested that the superheat plays a dominant role in flashing atomization, the synergistic mechanisms of these parameters remain to be thoroughly explored. What's more, for flashing spray studies, the typical medium are inert liquids, e.g., water and refrigerant, which has a significant gap in the thermo-physical properties of working

substance used in production applications. Besides, little concerns are given to the quantitative criterion for identifying flashing modes of superheated liquids, which is critical in preventing accidental release.

Therefore, the objective of this work is to investigate the underlying mechanism associated with the depressurization of iso-pentane. Here, a transparent straight nozzle is designed to produce the flashing spray, and the internal flow as well as external spray morphology are simultaneously captured via a high-speed camera. Subsequently, comprehensive experiments involving varying superheats and injection pressures are implemented for delivering the role of thermodynamic and mechanical effects on the flashing behaviors. To quantify the flashing modes, we propose a new index k to take into account both thermodynamic and mechanical effects. In addition, the microscopic characteristics, such as droplet diameter and velocity distributions, are also obtained by using a Phase Droplet Particle Analyzer (PDPA). And a new droplet diameter correlation is proposed for near-field and far-field regions. On the basis of this work, the experimental data is help to broaden the understanding of flashing spray characteristics and safety assessment in the superheated iso-pentane release.

2. Experimental system and methodology

2.1. Flashing spray system

Fig. 1 illustrates the experimental setup employed to visualize the internal flow and external flashing spray. The main system is comprised of a nitrogen cylinder, a 25 L pressure storage container, a control vessel, and a straight-tube nozzle. Here, iso-pentane is chosen as the research objective to simulate the accidental fuel emission. In experiments, the nitrogen cylinder connected with container can provide high pressure for driving iso-pentane into the control vessel. Meanwhile, a relief valve is equipped to adjust the injection pressure of control vessel. Then, the superheated liquids will pass through the solenoid valve, which controls the opening or closing by a home-made Labview program. In this experiment, the initial temperature of iso-pentane is regulated by a control vessel, where a heating unit is applied. More importantly, a transparent glass tube with length of 40 mm and inner diameter of 0.6 mm is adopted to clearly observe the internal flow pattern and primary breakup near the nozzle exist. Data acquisition board is employed to record signals and further synchronize the shooting of high-speed camera. Besides, to improve the experimental safety, an isolation hood and an exhaust fan are arranged to remove the harmful medium.

2.2. Imaging system and methodology

Based on back-illuminated imaging method, a high-speed camera (Fastcam SA-Z, Photron, Japan) is applied to obtain the transient images of internal flow pattern and external spray morphology. For that, a 120 W LED lamp served as the light source is located in the opposite of the high-speed camera, with the flashing spray in between. The sampling speed and maximum pixel resolution are 20,000 fps and 1024 × 1024 respectively to track the flow and spray evolution.

Taking initial temperature (T_{in}) of 70 °C and injection pressure (P_{inj}) of 0.9 MPa as an example, Fig. 2(a) shows the raw image of external flashing spray. In which, the black and white area represents the liquid and gas phase, respectively. It should be mentioned that as opposed to external observation, the liquid and bubble in the interior of nozzle represent white and black color respectively because of the reflection and refraction of light. To extract quantitative information from images, a Python-based code is developed to process the grayscale values. Here, a binarization method with threshold of 0.5 is used to obtain the peripheral part of flashing spray (Wang et al., 2023a), as shown in Fig. 2 (b). As well, the spray cone angle (θ) is defined to reflect the radial expansion in the near-field region. According to Eq. (1), θ is the function of spray width (D) and specified distance (L) from the nozzle. Besides, for each case, these values are averaged over 100 images after quasi-steady to minimize casual errors. In this work, each measure is repeated at least three times to estimate the experimental reliability. And the relative error in spray angle is within ±10 %. As seen in Fig. 2(c), owing to the grayscale differentiation, the raw image can be further transformed into pseudo-color image, which clearly reveals the spray morphology and droplet distribution.

$$\theta = 2\arctan\frac{D}{2L} \tag{1}$$

2.3. PDPA measurement

The droplet diameter and velocity were simultaneously measured using a phase droplet particle analyzer (PDPA by TSI, US). The PDPA is comprised of a laser-based optical transmitter, an optical receiver, and a signal processor. The specifications of PDPA system are listed in Table 1. During operating process, the optical transmitter produces four interfacing laser beams with two channel wavelengths of 514.5 nm and 488 nm. And the probe volume of laser beam is typically less than 1 mm^3. The Doppler signals and interface fringe patterns response correspondingly once droplets fly across the probe volume. As a result, the diameter and velocity distribution of droplets can be derived from the spatial

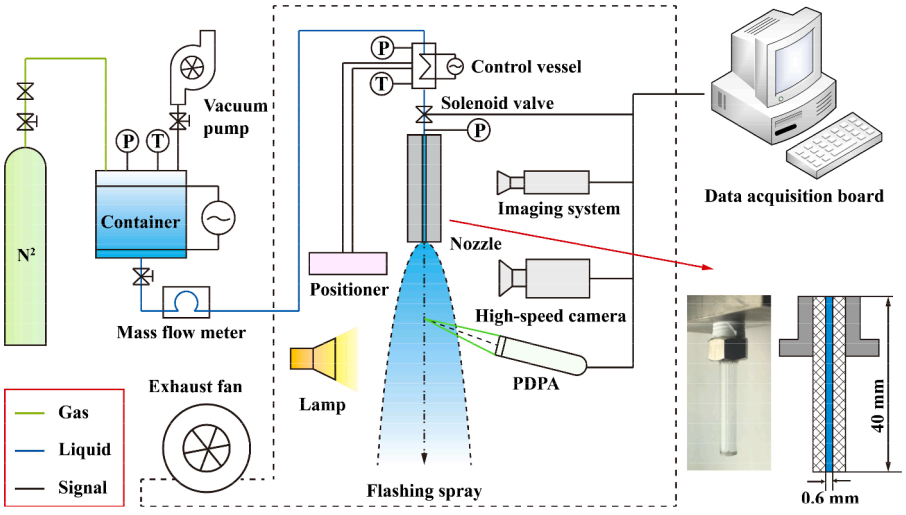

Fig. 1. Experimental setup for iso-pentane flashing spray.

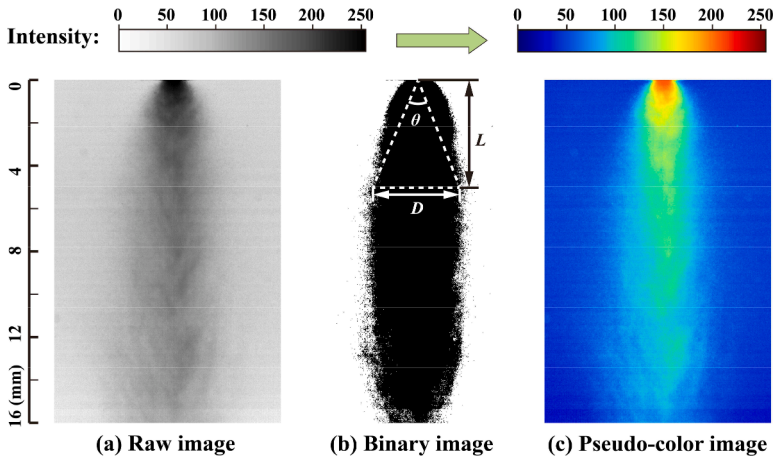

Fig. 2. Image post-processing procedure of flashing spray.

Table 1
Specifications of PDPA system.

Light source	Ar-ion laser
Wave length	514.5 nm, 488 nm
Beam diameter	2.8 mm
Focal length	250 mm
Expander ratio	1.0
Beam spacing	50 mm
Frequency shift	40 MHz
Scattering mode	Refraction
Receiver type	70 mm lens PDPA connected to 118 mm fiber
Laser power	800 mW

phase difference between the adjacent detectors and the frequency shift of Doppler signals, respectively. Besides, each measure is repeated at least three times to estimate the experimental reliability. The results show that the relative dispersions in droplet diameter and velocity are within ±3 and ±7 %, respectively.

2.4. Test conditions

To quantify the flashing release behaviors, iso-pentane is selected as the test fuel. In this study, the iso-pentane stored in a container is sub-cooled state and the ambient pressure (P_0) is maintained at 0.1 MPa. Fig. 3 depicts the saturation vapor pressure profile of iso-pentane. The normal saturation temperature of iso-pentane is about 27.8 °C under atmospheric pressure, which is easy to reach the superheated states. Typically, there are two approaches to change the subcooled liquid into superheated state and even activate flashing phenomenon, i.e., heating and depressurization. For this purpose, a wide range of superheated conditions are applied by changing the T_{in} from 40 to 80 °C and P_{inj} from 0.6 to 3.0 MPa, respectively. Here, a dimensionless number, known as superheat degree (R_p), is introduced to characterize the thermodynamic level caused by T_{in}. According to Eq. (2), R_p is described as the ratio between saturation pressure (P_s) at T_{in} and P_0. Notably, a high T_{in} of fuel will lead to a higher vapor pressure. More importantly, as shown in Eq. (3), R_p directly impact the chemical potential difference, which is the "generalized driving force" for phase transition. In which, k_b denotes the Boltzmann constant. For the superheated fuel, the chemical potential of liquid phase is obviously higher than that of vapor phase, thus driving the liquid-vapor phase transition (Wang et al., 2023a). So, R_p is used to assess the deviation from thermodynamic equilibrium in superheated liquids. Table 2 provides the values of R_p for test conditions. Besides, the bubble nucleation and the basic step of flashing, which can be described by Jacob number (Ja), as given in Eq. (4). In which, c_{pl} is the heat capacity of liquid, h_{fg} is the enthalpy for vaporization, ρ_l and the density of liquid phase, ρ_v is the density of vapor phase.

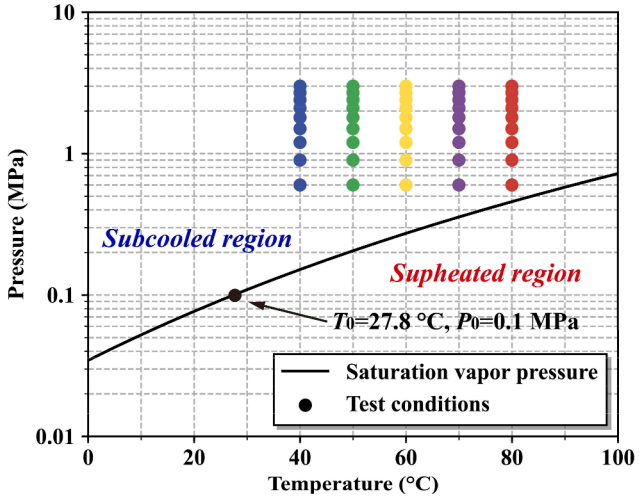

Fig. 3. Saturation vapor pressure of iso-pentane and test conditions.

$$R_p = \frac{P_s(T_{in})}{P_0} \tag{2}$$

$$\Delta\mu = \mu_l - \mu_v = k_b T_0 \ln(R_p) \tag{3}$$

$$Ja = \frac{c_{pl}\Delta T}{h_{fg}} \frac{\rho_l}{\rho_v} \tag{4}$$

In addition to the thermodynamic effect, the breakup of fuel spray is also related to mechanical forces. The relative extent of mechanical forces is usually expressed by Reynold number (Re), Weber number (We) and Ohnesorge number (Oh), which are formulated by Eqs. (5–7). Re and We describe the viscous force and the aerodynamic force, while Oh characterizes the jet properties and jet stability. In general, higher Oh indicates lower breakup probability of liquid jet.

$$Re = \frac{\rho_l d_0 u_{th}}{\mu_l} \tag{5}$$

Table 2
Values of the superheat degree R_p for test conditions.

R_p		T_{in} (°C)				
		40	50	60	70	80
P_0 (MPa)	0.1	1.51	2.06	2.73	3.56	4.57

$$We = \frac{\rho d_0 u_{th}^2}{\sigma} \tag{6}$$

$$Oh = \frac{\mu_l}{\sqrt{\sigma d_0 \rho_l}} \tag{7}$$

where d_0 is the hole diameter, u_{th} is the theoretical velocity inside the nozzle, μ_l is the liquid viscous force, σ is the surface tension. For accidental release of superheated fuel, the in-nozzle flow is more complicated due to phase transition. According to Bernoulli's equation, u_{th} can be determined by Eq. (8). It is noting that compared with single flow, the accidental release of superheated liquids involves complex phase change process. For this consideration, the discharge coefficient C_d is considered, which was proven to be 0.8 from previous study (Guo et al., 2021). Besides, Table 3 lists the thermo-physical properties of iso-pentane that are used in these equations.

$$u_{th} = C_d \sqrt{\frac{2\left(P_{inj} - P_0\right)}{\rho_l}} \tag{8}$$

3. Results and discussion

3.1. Macroscopic characteristics of internal flow and external spray

3.1.1. Effect of thermodynamic force on macroscopic characteristics

Fig. 4 shows the internal flow and external spray morphology of the quasi-steady stage for an injection pressure P_{inj} of 0.6 MPa with a superheat degree R_p ranging from 1.51 to 4.57. Results show that when the $R_p \leq 2.73$, an initial temperature below 60 °C, the internal flow morphology displays an almost transparent single-phase pattern without any bubble generation. Once increasing the superheat degree R_p to 3.56, a large number of bubbles are formed near the nozzle. At that time, the internal flow pattern shows the characteristics of two-phase bubbly flow. Then, fuel evaporation becomes obvious when the superheat degree R_p reaches 4.57, as shown in Fig. 4(e).

What's more, it should be mentioned that due to turbulence disturbance, the atomization quality for superheated liquid is highly affected by the cavitation extent. In general, two flashing locations can be distinguished, i.e., external flashing and internal flashing (Günther and Wirth, 2013). For external flashing, the bubble nucleation begins outside the nozzle. Then, the liquid jet is disrupted into ligaments due to bubble penetration and explosion. In contrary, internal flashing yields bubbles inside the nozzle, which directly contributes to the primary breakup near the outlet. In our results, it is evident that the entire structure of $R_p = 1.51$ is narrow and no distinct radical expansion happens along the jet direction. The reason is that when the superheated liquid is ejected into environment, the jet will be cooled by the surrounding air, which inhibits the liquid from being superheated state and suppresses flashing atomization. As a result, despite the iso-pentane is pre-superheated, the non-flashing mode is primarily driven by the mechanical effect (difference between injection pressure and ambient pressure), while the thermodynamic effect at low R_p is too weak to disintegrate the liquid. However, the internal flashing is emerged when R_p increases to 2.06 and 2.73, indicating the thermodynamic effect is sufficient to withstand the cooling. In this case, droplet clusters and earlier breakup are formed under the conjugated action of mechanical and thermodynamic effects. The superheated jet is shattered into not well-atomized liquid ligaments, which corresponds to the transitional flashing mode. Notably, the flashing spray can provide a finer droplet size distribution once $R_p \geq 3.56$. As well, intense visible in-nozzle bubbles are generated and then burst to disperse the liquid jet at the near-field region, resulting in internal flashing. These results means when P_{inj} is unchanged, the thermodynamic effect driven by superheat plays an essential role in promoting droplet atomization during flashing conditions.

Table 3
The thermo-physical properties of iso-pentane in temperature range of 300–400 K.

Properties	Unit	Relations
ρ_l	kg m^{-3}	$6.303 \times 10^2 + 0.826T - 2.953 \times 10^{-3}T^2$
ρ_v	kg m^{-3}	$2.709 \times 10^2 - 1.796T + 3.016 \times 10^{-3}T^2$
c_{pl}	J kg^{-1} K^{-1}	$3.404 \times 10^3 - 11.784T + 2.691 \times 10^{-2}T^2$
μ_l	Pa s	$1.367 \times 10^{-3} - 5.759T + 6.387 \times 10^{-9}T^2$
σ	N m^{-1}	$5.552 \times 10^{-2} - 1.665 \times 10^{-4}T + 9.639 \times 10^{-8}T^2$
h_{fg}	J kg^{-1}	$2.119 \times 10^5 + 1.501 \times 10^3 T - 3.632T^2$

3.1.2. Effect of mechanical force on macroscopic characteristics

Although thermodynamic effect has a pronounced impact at high superheat, the mechanical effect is also believed to be important for the spray structure by enhancing the inertial force. Fig. 5 shows the effect of P_{inj} on spray morphology of iso-pentane with $R_p = 1.51$. It is noting that evaporation is not observed inside the nozzle for all cases due to poor superheat degree. Notably, when the P_{inj} is low, the boundary of superheated jet is relatively smooth, and the spray pattern exhibits jet impingement behavior in non-flashing mode, as seen in Fig. 5(a) and (b). Then, the spray cone angle gradually expands and the liquid core is spitted into micro-explosion droplets as P_{inj} increases to above 1.8 MPa. Such phenomenon is attribute to the enhancement of mechanical effects. For one point, the jet velocity increases as a function of square root with respect to P_{inj}. When the changes of temperature-induced properties can be ignored, the values of *Re* and *We* are dependent on the velocity, according to Eqs. (4) and (5). This indicates that the jet instability would increases at higher P_{inj}, leading to the improvement in breakup possibility of droplet during flashing spray. For another point, the aerodynamic forces induced by the interaction between fuel jet and air flow are also enhanced. As a result, the external flashing driven by high P_{inj} is responsible for a more intensified breakup process of droplets.

3.1.3. Coupling effect on macroscopic characteristics

The above results reveal that the morphology and atomization of superheated fuel is concerned by the coupling of thermodynamic and mechanical effects. The deep interaction between these two effects can be revealed from the perspective of bubble breakup model. For a bubble-droplet system, the breakup would occur when the amplitude of surface disturbance and the thickness of liquid layer reaches a certain characteristics length (Gao et al., 2020). In other words, the liquid layer will break up if the surface tension of outer layer fails to resist the disruptive action from mechanical effects, like inertial and aerodynamic forces. In addition, driven by thermodynamic effect, the vapor escaping from bubble generates burst energy, which further leads to an explosive flashing breakup. The work of Zhu et al. (2023a) is worth mentioning, in which the relationship between thermodynamic effect (E) and mechanical effect (ω) is expressed by

$$E \propto \phi^2 J \left(\frac{2\sigma}{P_s - P_0} + 2Ja \sqrt{\frac{3\lambda_l}{\pi \rho_l c_{pl}}} \sqrt{\frac{12}{\omega}} \right)^2 \tag{9}$$

where ϕ is the spray diameter that can be approximated by d_0, J is the nucleation rate that keeps constant for a given T_{in}, λ_l is the thermal conductivity of liquid phase, c_{pl} is the thermal capacity of liquid phase. E is the bubble burst energy caused by thermal nonequilibrium, and ω is the instability growth rate for bubbles and disturbances, indicating the intensity of mechanical effect. Based on linear stability analysis, the theorical ω is derived by analytically or numerically solving a multivariable cubic equation (Lv et al., 2012). Lü et al. (2015) built a mathematical model to explore the instability of cavitation bubbles. It was found that the value of ω was increased corresponding as the velocity increased. Assuming T_{in} and d_0 are unchanged during adiabatic expansion process, the lower velocity implies a smaller ω, followed by an increase in E. It should note that the practical flashing process is far

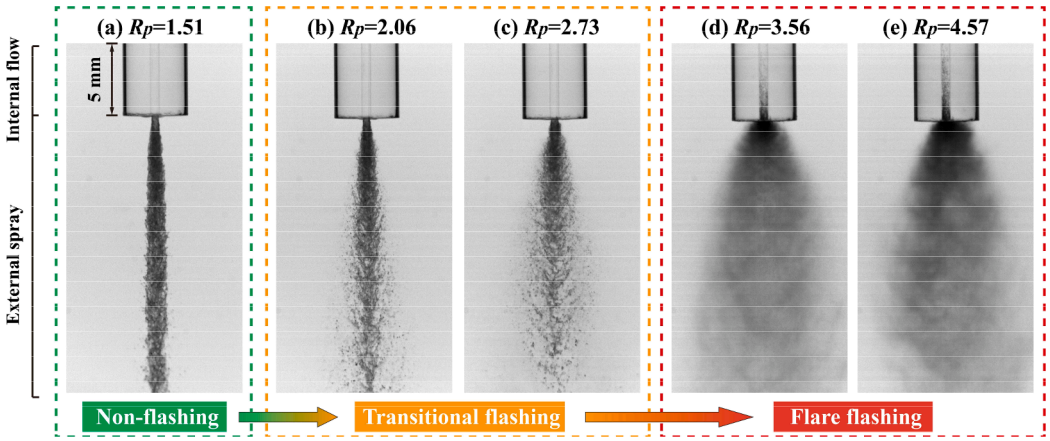

Fig. 4. The stable internal flow and external spray morphology of iso-pentane at P_{inj} = 0.6 MPa with increasing superheat degree.

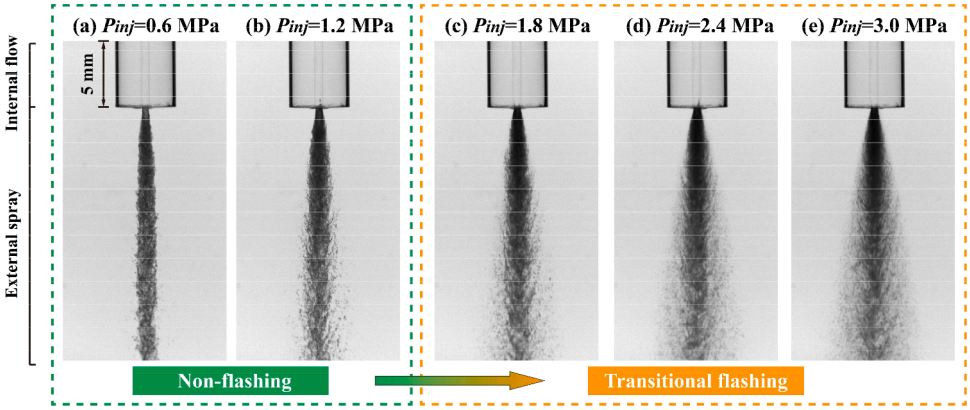

Fig. 5. The stable internal flow and external spray morphology of iso-pentane at R_p = 1.51 with increasing injection pressure.

beyond the adiabatic expansion assumption. Compared to the breakup of subcooled jet, the underlying mechanisms of flashing jet are more complicate due to the presence of phase changes. Li et al. (2017) found that the droplet breakup was associated with a critical superheat degree above which the dominant breakup mechanism shifted from aerodynamic mode to thermodynamic mode. From these results, it can be speculated that increasing mechanical effect decreases the contribution of thermodynamic effect in flashing spray because of shortening the bubble nucleation time and reducing the vapor volume to burst.

Figs. 6 and 7 further presents the external spray morphologies and core angle of all test conditions under quasi-steady stage. Depending on the intensity of breakup and dispersion cone angle, the flashing patterns can be described by three modes, namely non-flashing, transitional flashing, and flare flashing (Wang et al., 2023a; Zhu et al., 2023a). For non-flashing spray, the intensity of droplet breakup is weak and cannot shatter the jet when R_p and P_{inj} are low. However, when P_{inj} increases to 1.2 MPa, the inertial and aerodynamic forces at R_p of 1.51 are sufficient to facilitate the dispersion of droplets surrounding the main jet, leading to transitional flashing spray. Although flashing behavior is prominent, this mode is characterized by large undispersed sub-jets. This suggests that the mechanical effect is still the important factor to induce breakup, while the thermodynamic effect is responsible for assisting the breakup through bubble blast. When R_p is as high as 2.73, the continuous liquid cores are almost invisible and the completely atomization is appeared at the near-field region under P_{inj} = 2.1 MPa, indicating the onset of flare flashing. In this mode, the superheated spray driven by internal flashing performs a remarkably radial expansion with large cone angle, as shown in Fig. 7. The further increase in R_p can enhance the in-nozzle bubble nucleation and droplet formation, but the flashing spray structure has no significant variation.

3.2. *Determination of flashing regions*

To clearly interpret the dynamic behaviors of flashing spray, Fig. 8 summarizes the schematic of flashing mechanism in terms of superheats and the macroscopic morphologies under different conditions. Based on the experimental observations, both mechanical effect and thermodynamic effect have significant influences on the spray structure and atomization. The former involves aspects like surface tension, aerodynamic drag, etc., while the latter is related to the bubble nucleation and explosion. When superheat is low, the cooling air prevents the appearance of flashing, leading to non-flashing mode. At that time, the spray jet breakup is controlled by mechanical effect. Following, with the superheat increases into transitional region, the thermodynamic effect is sufficient to overcome the ambient cooling and contributes to flash boiling. As shown in Fig. 8(c), for transitional flashing, the bubble nucleation, collision, and aggregation are occurred near the nozzle exit. When the superheat exceeds the critical level of surface tension, a bubble burst phenomenon begins to initiate jet disintegration, leading to a narrow liquid core and large droplets. Further increasing the superheat promotes the formation of in-nozzle bubble, as illustrated in Fig. 8(d). For flare flashing, the jet at near-nozzle regime fully atomizes into well-dispersed fine droplets as soon as the superheated fuel is ejected into environment. In this condition, only an extremely thin liquid core can be identified and a wider spray structure is obtained.

For the prevention of accidental release, the vital objective is not only to identify the dynamic characteristics of flashing jet, but also to establish a proper criterion for predicting the flashing mode of super-

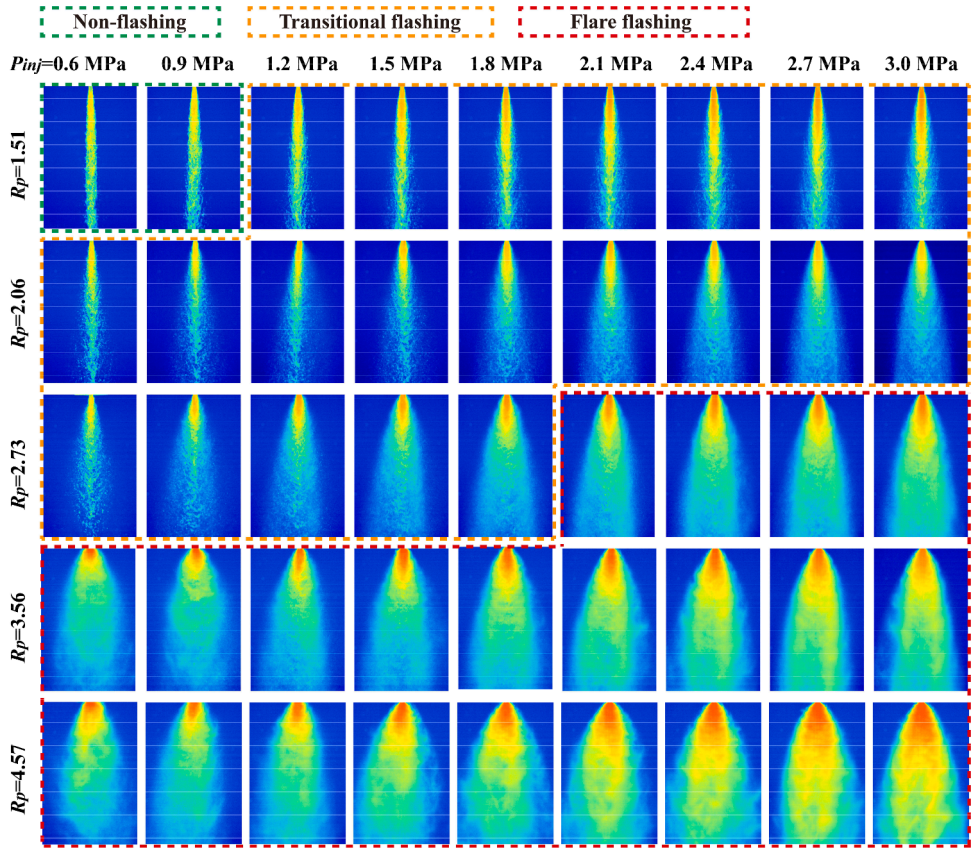

Fig. 6. Pseudo-color images for external spray morphology of iso-pentane at superheat degree R_p of 1.51–4.57 and injection pressure P_{inj} of 0.6–3.0 MPa.

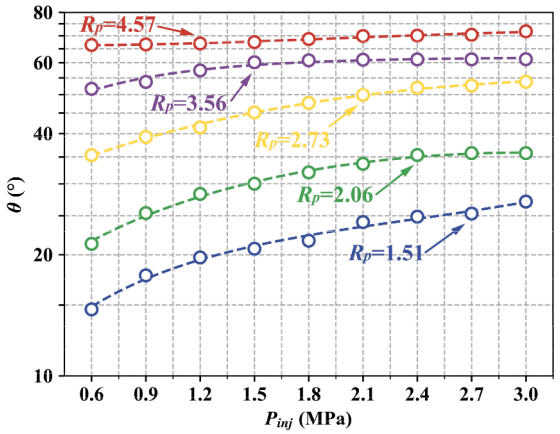

Fig. 7. Cone angle of flashing spray under different test conditions.

heated fuel. On this basis, it is possible to assess the accident risk and further elaborate the subsequent migration procedures. Up to the present, however, limited attentions have been paid to the development of quantitative criterion. Here, five typical criterions are illustrated in Eqs. (10–14), which provide a valuable reference for constructing a suitable criterion for distinguish the flashing mode of iso-pentane fuel.

(1) Zeng et al. (2012) classified the spray behavior of alcohol fuel into three states in terms of R_p values. A subcooled spray is defined as $R_p<1$, which only produces liquid jet. Then, when R_p is between 1 and 3.3, the fuel spray enters into transitional state, which indicates the enhancement of flashing atomization. Once R_p exceeds 3.3, due to the high vapor pressure, a dramatic evaporation and a collapse structure of fuel spray will occur, which is referred as the flare state. The corresponding criterion can be expressed by

$$\begin{cases} R_p < 1 & \text{Non}-\text{flashing} \\ 1 \le R_p < 3.3 & \text{Transitional}-\text{flashing} \\ R_p \ge 3.3 & \text{Flare}-\text{flashing} \end{cases} \tag{10}$$

(2) By reverting the nucleation theory, Lamanna et al. (2014) proposed a non-dimension expression to specify the energy barrier for flare flashing, as given below.

$$\chi = \frac{\Delta G}{k_b T_{in}} = \frac{16\pi\sigma^3}{3(\Delta\mu)^2} \begin{cases} \chi < 1 & \text{Flare}-\text{flashing} \\ 1 \le \chi < 4 & \text{Onset} \\ \chi \ge 4 & \text{Beforeonset} \end{cases} \tag{11}$$

where χ is the ratio between bubble nucleation energy and chemical potential difference, ΔG is the formation energy to create a critical bubble cluster. The excess in chemical potential is sufficient to offset the work for forming new surface when $\chi<1$, thus accelerating the transition to flare flashing.

(1) Zalkind et al. (2021, 2019) also established a criterion to determine the reaching of water flare flashing, as formulated in Eq. (12).

$$K_s = \frac{3(1-1/R_p)}{2\ln(R_p)} \begin{cases} K_s < 0.6 & \text{Non}-\text{flashing} \\ 0.6 \le K_s < 0.8 & \text{Transitional}-\text{flashing} \\ K_s \ge 0.8 & \text{Flare}-\text{flashing} \end{cases} \tag{12}$$

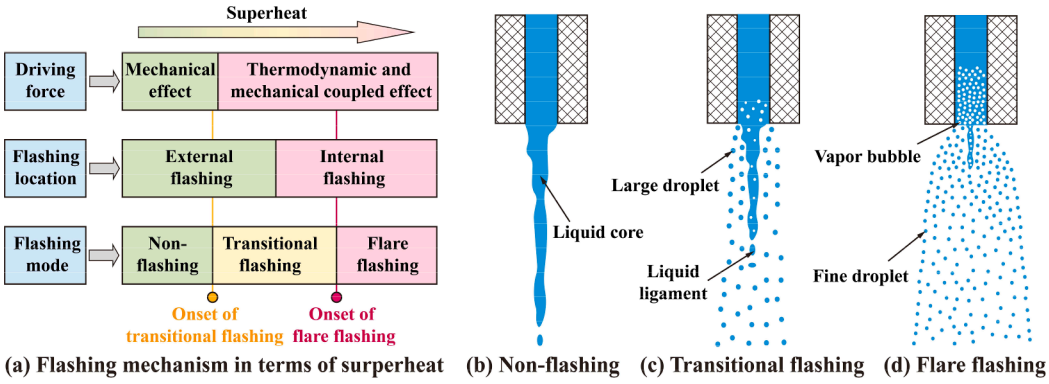

Fig. 8. Schematic of flashing mechanism and spray characteristics under different conditions.

where K_s is the ration between surface tension energy and chemical potential energy of vapor mass in critical cluster.

(1) To judge the flashing mode of water, Cleary et al. (2007) and Witlox et al. (2007) developed an empirical model, which considered droplet distribution and jet structure. The model predicts the evolution of drop size with increasing superheat, as shown in Eq. (13).

$$Ja\varphi = kWe_v^{-1/7}\begin{cases} k < 55 & \text{Non}-\text{flashing} \\ 55 \le k < 150 & \text{Transitional}-\text{flashing} \\ k \ge 150 & \text{Flare}-\text{flashing} \end{cases} \tag{13}$$

where $\varphi = 1 - \exp(-2300\rho_v/\rho_l)$ is a correction factor, evaluating the ratio between vapor and liquid density at T_{in}. In this model, the thermodynamic effect and mechanical effect are represented by bubble growth ($Ja\varphi$) and aerodynamic force ($kWe_v^{-1/7}$), respectively.

(1) Recently, Zhu et al. (2023b) provided a modified criterion to distinguish the flashing mode of water. Based on Eq. (14), the contribution of thermodynamic (JaR_p) and mechanical (We_vOh) effects are coupled.

$$JaR_p = k(We_vOh)^{-1/7}\begin{cases} k < 41 & \text{Non}-\text{flashing} \\ 41 \le k < 233 & \text{Transitional}-\text{flashing} \\ k \ge 233 & \text{Flare}-\text{flashing} \end{cases} \tag{14}$$

To enhance the understanding, Fig. 9 shows the classification of the present test conditions following these criterions for distinguishing the flashing modes of iso-pentene. In which, the solid line marks the threshold for non-flashing and transitional flashing, and the dash line denotes the limit for onset of flare flashing region. Particularly, the liquid properties are estimated at T_{in}, while the vapor properties are taken at the atmospheric saturation state. And the x-axis ticks are set to We_v for Eqs. (10–12), which only involves the thermodynamic effect. It is noting that high superheat indicates high R_p, low χ, and low K_s. For Eq. (10), the experimental points are located properly in the corresponding flashing region. But without the mechanical effect, the limits of flashing regions cannot be well identified. As seen in Fig. 9 (b and c), Eqs. (11 and 12) obviously underestimate the thermodynamic effect that are required to achieve the transitional flashing and flare flashing. The reason can be explained that the working mediums in the studies of Lamanna et al. (2014) and Zalkind et al. (2021, 2019) were acetone and water, respectively, which require relatively larger R_p to trigger flash-boiling due to their higher atmospheric boiling point than iso-pentane. According to experimental analysis, mechanical effect has an essential influence on the jet breakup, especially in non-flashing and

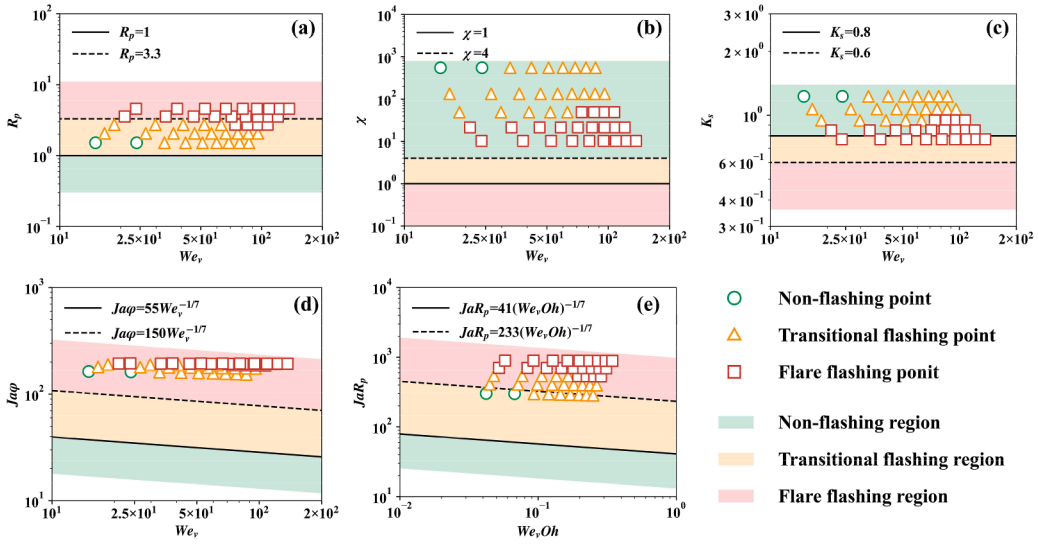

Fig. 9. Criterion for distinguishing the flashing modes of different test conditions according to Eqs. (10–14).

transitional flashing regions. For Eq. (13) involving the aerodynamic force (We_v), however, the model still overestimates the onset of flashing mode of iso-pentane. It indicates that simply integrating Ja and We_v is insufficient to reflect the coupling actions between thermodynamic and mechanical effects. Note that Eq. (14) further considers the R_p and Oh, which represent the extent of phase change and jet stability, respectively. It is noticed from Fig. 9(e) that despite the points are over the transitional region, the model shows a great potential to classify the flashing modes, as the tendency agrees well with test conditions.

The above results show that the existing criterions can predict the flashing modes of iso-pentane to some extent. However, most of the working fluids are focused on high-boiling substances such as water, whose thermo-physical properties are far different from industrial fuels. More importantly, the coupling interaction between thermodynamic and mechanical effects is also required to be considered. In order to facilitate the application of these criterions to iso-pentane fuel, a further modified relationship is particular required. Inspired by previous criterions, the driving forces denoting thermodynamic and mechanical effects can be degenerated to the groups of $f(Ja,\ R_p)$ and $f(We_v,\ Oh)$, respectively. So, the quantitative criterion coupling these two driving forces in this work take the same form as the one originally proposed by Zhu et al. (2023b), but with new constants developed. The generalized form of criterion is expressed by

$$f\left(Ja, R_p\right) \propto f\left(We_v, Oh\right) \tag{15}$$

$$Ja^{n_1} R_p^{n_2} = kWe_v^{n_3} Oh^{n_4} \tag{16}$$

Nevertheless, determining the coefficients for this explicit equation is difficult because of the wide range of parameters. For this consideration, the coefficients of Ja, R_p, We_v, and Oh among Eq. (14) are directly cited in this work. And two limits (k) that classifies the flashing boundaries are proposed empirically. Hence, the modified criterion for the onsets of transitional and flare flashing is shown in Eq. (17). Note that this criterion is consistent for the present test conditions of iso-pentane, as shown in Fig. 10. To illustrate the validity of this criterion, the data obtained from Soo Yu et al. (2023) and Rees et al. (2020) are also displayed. It is observed that this criterion shows well agreement with the results of n-heptane and n-butane, but it predicts flashing onset of liquid nitrogen early due to the difference in material properties. To sum up, the modified criterion can be applied to evaluate the contribution of thermodynamic and mechanical effects during flashing process. When $k < 212$, $212 \le k < 425$, $k \ge 425$, the external spray pattern undertakes a non-flashing, transitional flashing, and flare flashing modes. In addition, the equation also confirms that decreasing mechanical effect (We_vOh) leads to an increase in thermodynamic effect (JaR_p), which is evidenced by Eq. (9).

$$JaR_p = k(We_vOh)^{-1/7} \begin{cases} k < 212 & \text{Non} - \text{flashing} \\ 212 \le k < 425 & \text{Transitional} - \text{flashing} \\ k \ge 425 & \text{Flare} - \text{flashing} \end{cases} \tag{17}$$

3.3. Microscopic characteristics of droplets

The dynamic jet characteristics, such as arithmetic average velocity and droplet Sauter mean diameter (D_{32}), are investigated under a fairly wide range of T_{in} and P_{inj}. Here, total 140 sampling points are taken along the axial direction (Z) to detect the statistic information, with effective droplet count of 6000 at least. However, due to the dense size distribution at near-field region, getting the details of droplets accurately is difficult. Out of this concern, the shortest test position is set at Z = 20 mm. For all cases, the obvious Gaussian velocity and Rosin–Rammler D_{32} distributions are noticed. One example with T_{in} = 50 °C, P_{inj} = 2.1 MPa, and Z = 100 mm is shown in Fig. (11).

3.3.1. Droplet velocity distribution

Fig. 12 shows the evolution in arithmetic average velocity of droplets on the centerline of spray jet. As illustrated in Fig. 12(a), the droplet velocities exhibit the same decreasing trend with flying forward. When T_{in} rises to 50 °C, the velocity increases at the near-field region and then decreases slowly at the far-field region, as shown in Fig. 12(b). This is due to that the droplets undergoes more drag force near nozzle exit, causing a sharp deceleration. However, the droplet peak velocity has no significant change after further elevating T_{in}, as depicted in Fig. 12 (c and d). As compared to the upstream of low T_{in}, the high fluctuation at high superheat can be related to the dense droplet concentration at near-field region, which leads to more stronger collisions. Besides, the droplet velocity is obviously increased with the improvement of P_{inj}. It is expected that the release rate of superheated liquid accelerates at high P_{inj} because of the large pressure difference between container and environment. For the cases of T_{in} = 40 °C and T_{in} = 50 °C, the droplet velocity is directly affected by the change of P_{inj} because mechanical effect has a predominant role in the non-flashing and transition flashing modes. By increasing P_{inj}, the higher kinetic energy would drive the droplet to atomize and fly forward at a high velocity. When $T_{in} \ge 60$ °C, the regularity of droplet velocity becomes complex due to the coupling interaction between mechanical and thermodynamic effects. The high P_{inj} provides higher flow rate, whereas less bubble and void fraction would form inside the nozzle. More importantly, the internal flow pattern has an essential effect on fluid velocity and further influence the flashing structure. Therefore, the droplet velocity has a negative relation to the P_{inj} under high superheat conditions.

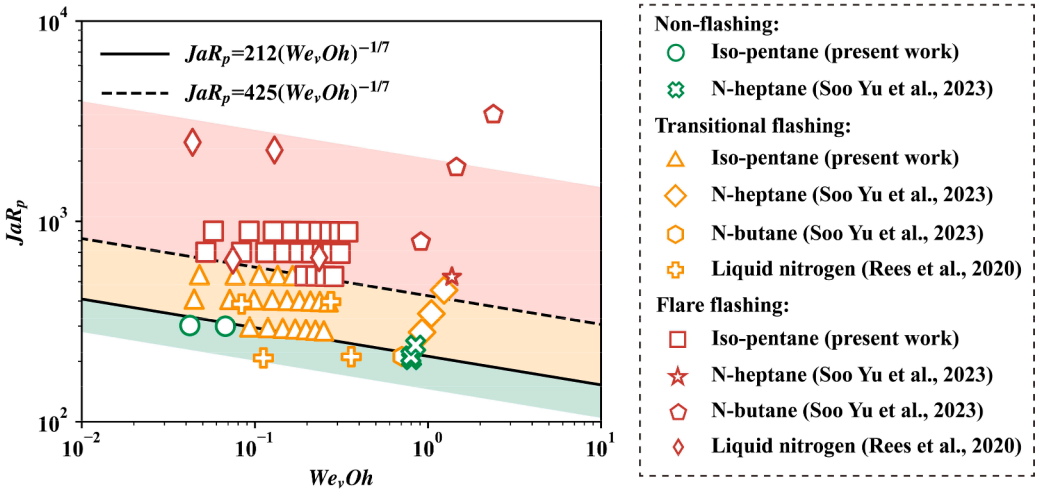

Fig. 10. Criterion for distinguishing the flashing modes of different test conditions according to Eqs. (17 and 18).

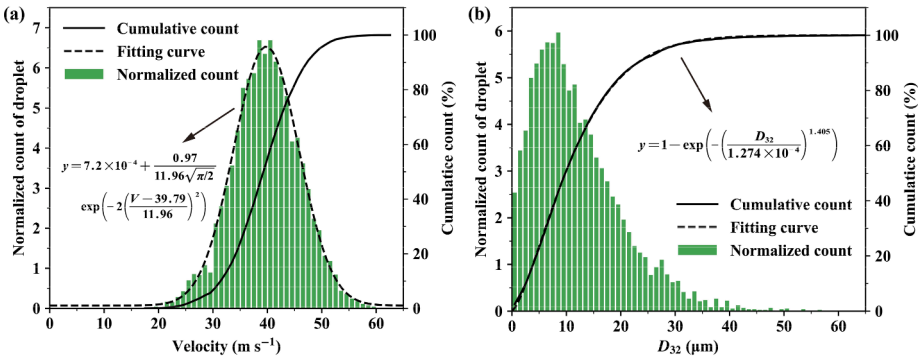

Fig. 11. Distribution of (a) average velocity and (b) droplet diameter for the case of T_{in} = 50 °C and P_{inj} = 2.1 MPa at axial distance Z = 100 mm.

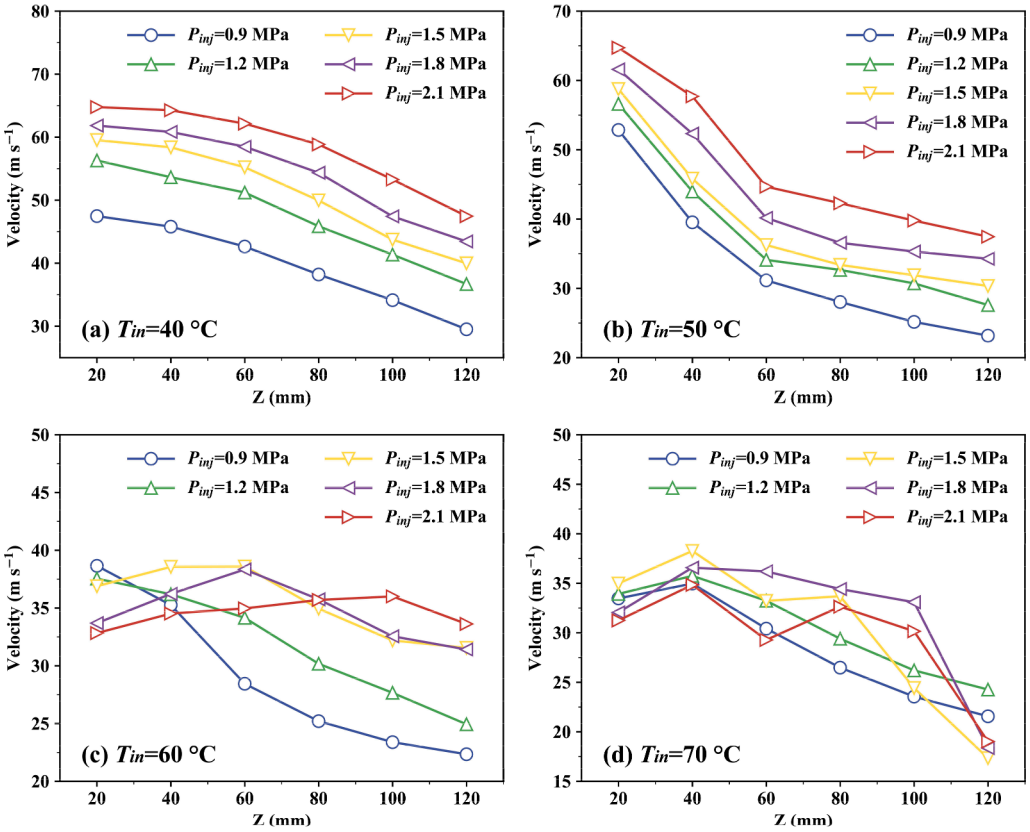

Fig. 12. Evolution of droplet velocity under different initial temperature and injection pressure.

3.3.2. *Droplet diameter distribution*

The corresponding diameter of iso-pentane droplets along axial direction is shown in Fig. 13. It is noting that the D_{32}, knows as the volume/surface ratio of total droplets at test point, is a representative index to evaluate the extent of atomization quality and evaporation. Obviously, drop size presents a sharp reduction as increasing axial distance within the first 40 mm. The reason is attributed to the flashing atomization of droplets caused by a sudden depressurization. As shown in Fig. 12(a), when T_{in} < 50 °C, the liquid ejects into ambient through nozzle has not been broke up completely, resulting in large size of droplets. And the drop size continues to decreases along axial direction due to the dominance of mechanical effect like flow instability and turbulence disturbance. On the other hand, when the $T_{in} \geq$ 50 °C, the jet becomes superheated state and then breaks up strongly because of the thermodynamic non-equilibrium effect including evaporation and boiling. Following, the droplets undergo a quick phase change process and remain relatively stable once the excess energy is released through explosive atomization. Yildiz et al. (2002) owed this stable diameter distribution to the mono-dispersed spray as it flying further away from nozzle. Besides, the whole variation of droplet diameter shows a decrease trend as the P_{inj} increases. The possible reason is that the drop size at low P_{inj} is mainly affected by the individual large droplet, while it may be well atomized and towards a more uniform distribution with increasing P_{inj}. As a result, the diameter gradually gets rid of the dependence from large droplets at high P_{inj}.

3.3.3. *Correlation of droplet diameter*

The measurement locations for droplet diameter have been discussed in previous part. However, in order to derive the atomization in relation to release conditions, a droplet diameter correlation for a global SMD is helpful to reflect the changing rates across the spray. Cleary et al. (2007) proposed a droplet SMD correlation, where SMD was taken from We_l, Re, and nozzle aspect ratio (L/d_0). Note that the effect of orifice diameter on flashing spray characteristics is not taken into account. For this

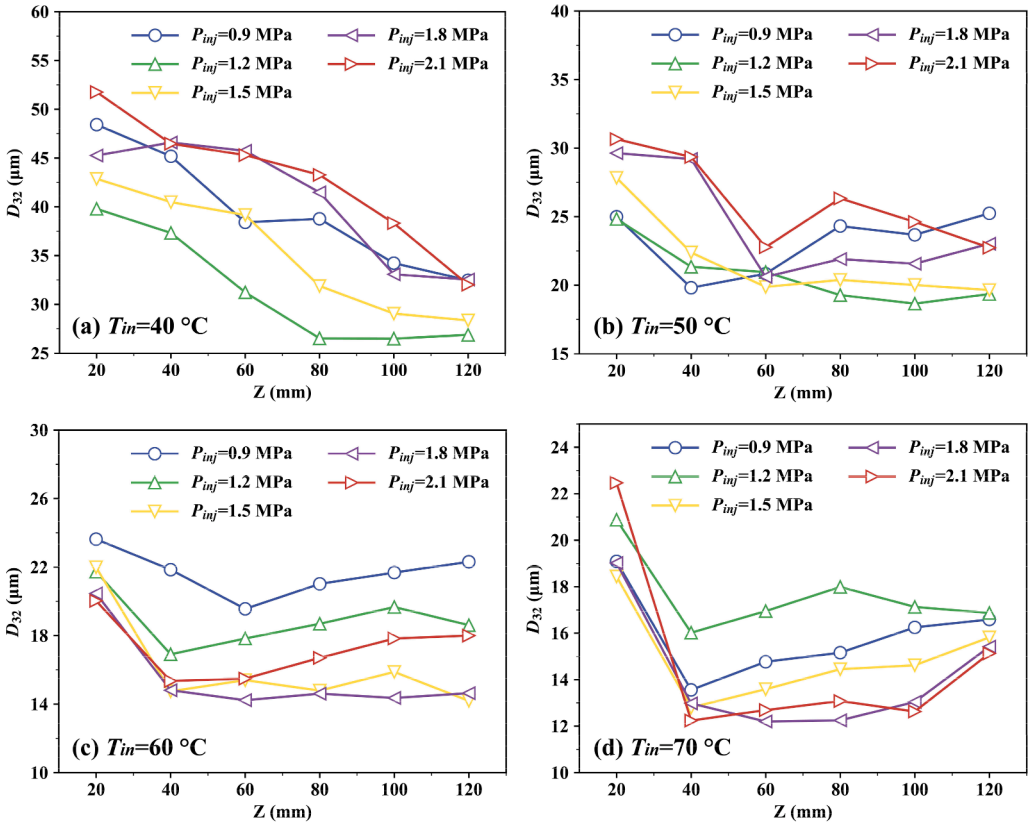

Fig. 13. Evolution of droplet diameter under different initial temperature and injection pressure.

consideration, the coefficient of (L/d_0) proposed by Cleary et al. (2007) is cited here. Eq. (18) presents the correlation $f(We_l, Re, L/d_0)$ for the experimental results of iso-pentane. In this correlation, the influencing factors of droplet SMD is only explained by mechanical-breakup criterion, which is inadequate to describe the flashing atomization. On this basis, the SMD correlation should further take into account the thermodynamic effects, including R_p and Ja. Here, the global SMD is determined at the position of $Z = 20$ mm and $Z = 120$ mm, aiming to represent the SMD behavior at near-field and far-field regions. As seen in Eq. (19), the new SMD correlation for flashing releases is formulated into the non-dimensional groups. In addition, the SMD correlations that only considers mechanical forces are also derived. Fig. 14 shows the variation of experimental and predicted SMD via different correlations. It is observed that the previous correlation $f(We_l, Re, L/d_0)$ has significant deviation for the measured results. After involving the thermodynamic factors, the new correlation $f(We_l, Re, L/d_0, Ja, R_p)$ presents a better accuracy with relative deviation less than 20 and 25 % at axial direction of 20 and 120 mm, respectively.

$$\frac{D_{SMD}}{d_0} = \begin{cases} 14We_l^{0.26}Re^{-0.92}\left(\frac{L}{d_0}\right)^{0.114} & Z = 20\text{mm} \\ 27We_l^{0.19}Re^{-0.95}\left(\frac{L}{d_0}\right)^{0.114} & Z = 120\text{mm} \end{cases} \tag{18}$$

$$\frac{D_{SMD}}{d_0} = \begin{cases} 75We_l^{0.49}Re^{-0.84}\left(\frac{L}{d_0}\right)^{0.114}Ja^{-0.69}R_p^{-0.99} & Z = 20\text{mm} \\ 64We_l^{0.17}Re^{-0.54}\left(\frac{L}{d_0}\right)^{0.114}Ja^{-0.75}R_p^{-0.71} & Z = 120\text{mm} \end{cases} \tag{19}$$

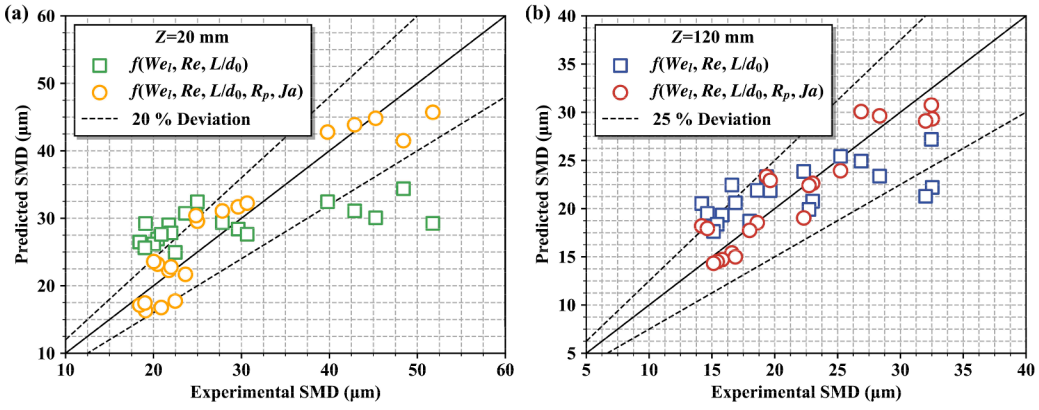

Fig. 14. Comparison of experimental SMD and predicted SMD for different correlations.

4. Conclusions

In this study, the flashing behaviors of iso-pentane are experimentally explored from the perspective of internal flow and external spray. Here, the analysis focuses on the key parameters of T_{in} and P_{inj} in the range of 40–80 °C and 0.6–3.0 MPa. Results show that the characteristics of flashing spray is affected by the coupling of mechanical effect and thermodynamic effect. Mainly conclusions are drawn below:

- According to breakup intensity, flashing spray is classified into three modes, i.e., non-flashing where the flashing intensity is weak and cannot shatter the jet, transitional flashing where a narrow liquid core and large droplets begins to occur, and flare flashing where only extremely small liquid core is identified.
- Higher R_p contributes to bubble formation inside nozzle, thus enhancing flashing atomization. When R_p is low, the inertial and aerodynamic forces at higher P_{inj} facilitates the dispersion of droplets. What's more, increasing thermodynamic effect can decrease the contribution of mechanical effect in breakup of flashing jet.
- A quantitative criterion of $JaR_p = k(We_vOh)^{-1/7}$ is recommended to determine the flashing mode, where $k < 211$, $212 \leq k < 425$, and $k \geq 425$ corresponds to the non-flashing, transitional flashing, and flare flashing regions, respectively.
- For droplet velocity, the role of thermodynamic effect in far-field region is gradually reduced as Tin increases. And high P_{inj} provides high flow rate, leading to less in-nozzle bubble and void fraction. So, the droplet velocity is negatively associated with P_{inj} under high superheats.
- A new SMD correlation $f(We_l, Re, L/d_0, Ja, R_p)$ is developed to derive the atomization in relation to release conditions. It is expected to examine the drop size behaviors at near-field and far-field regions.

CRediT authorship contribution statement

Xiang-Wei Lin: Investigation, Methodology, Software, Writing – original draft, Writing – review & editing. **Dong-Qing Zhu:** Methodology, Writing – original draft. **Zhi-Fu Zhou:** Conceptualization, Supervision, Funding acquisition, Writing – review & editing, Validation. **Shu-Qin Xue:** Investigation. **Teng-Fei Liu:** Validation. **Jia-Feng Wang:** Data curation, Validation. **Bin Chen:** Supervision, Funding acquisition. **Eric Lichtfouse:** Writing – review & editing.

Declaration of Competing Interest

The authors declare that they have no known competing financial interests or personal relationships that could have appeared to influence the work reported in this paper.

Data availability

Data will be made available on request.

Acknowledgements

We sincerely acknowledge the support from National Natural Science Foundation of China (52176163), the Ministry of Science and Technology of Shaanxi province of China (2023-YBGY-379), and Fundamental Research Funds for the Central Universities. The corresponding author (Z.-F. Zhou) as a "Tang Scholar" greatly appreciates the support from the Cyrus Tang Foundation.

Reference

Allen, J., 1998. Laser-based measurements in two-phase flashing propane jets. Part two: droplet size distribution. J. Loss Prev. Process Ind. 11 (11), 299–306.
Allen, J.T., 1988. Laser-based measurements in two-phase flashing propane jets. Part one: velocity profiles. J. Loss Prev. Process Ind. 11 (5), 291–297.
Brown, R., York, J.L., 1962. Sprays formed by flashing liquid jets. AIChE J. 8, 149–153.
Cleary, V., Bowen, P., Witlox, H., 2007. Flashing liquid jets and two-phase droplet dispersion I. Experiments for derivation of droplet atomisation correlations. J. Hazard. Mater. 142, 786–796.
Gao, X., Bao, S., Shao, S., Hu, H., Zhou, S., Chen, J., Xie, J., 2020. Theoretical analysis on the atomization characteristics of liquid nitrogen jets. Phys. Fluids 32, 054102.
Günther, A., Wirth, K.E., 2013. Evaporation phenomena in superheated atomization and its impact on the generated spray. Int. J. Heat Mass Transf. 64, 952–965.
Guo, H., Li, Y., Lu, X., Zhou, Z., Xu, H., Wang, Z., 2019a. Radial expansion of flash boiling jet and its relationship with spray collapse in gasoline direct injection engine. Appl. Therm. Eng. 146, 515–525.
Guo, H., Li, Y., Xu, H., Shuai, S., Zhang, H., 2019b. Interaction between under-expanded flashing jets: a numerical study. Int. J. Heat Mass Transf. 137, 990–1000.
Guo, X., Tan, W., Liu, L., Liu, C., Zhu, G., 2021. Experimental study of liquefied gas dynamic leakage behavior from a pressurized vessel. Process Saf. Environ. Prot. 151, 20–27.
Hervieu, E., Veneau, T., 1996. Experimental determination of the droplet size and velocity distributions at the exit of the bottom discharge pipe of a liquefied propane storage tank during a sudden blowdown. J. Loss Prev. Process Ind. 9 (6), 413–425.
Hwang, J., Yasutomi, K., Arienti, M., Pickett, L.M., 2020. Numerical Investigation of Near Nozzle Flash-Boiling Spray in an Axial-Hole Transparent Nozzle. SAE Technical Paper Series.
Ji, R.-J., Zhu, D.-Q., Lin, X.-W., Zhou, Z.-F., Chen, B., 2023. Parametric investigation on the close-loop R410A flash spray system for high power electronics cooling under low temperature. Case Stud. Therm. Eng. 41, 102643.
Jing, D., Zhang, F., Li, Y., Xu, H., Shuai, S., 2017. Experimental investigation on the macroscopic and microscopic spray characteristics of dieseline fuel. Fuel 199, 478–487.
Lamanna, G., Kamoun, H., Weigand, B., Steelant, J., 2014. Towards a unified treatment of fully flashing sprays. Int. J. Multiphase Flow 58, 168–184.
Li, S., Zhang, Y., Qi, W., Xu, B., 2017. Quantitative observation on characteristics and breakup of single superheated droplet. Exp. Therm. Fluid Sci. 80, 305–312.
Li, Y., Guo, H., Zhou, Z., Zhang, Z., Ma, X., Chen, L., 2019. Spray morphology transformation of propane, n-hexane and iso-octane under flash-boiling conditions. Fuel 236, 677–685.
Loureiro, D.D., Kronenburg, A., Reutzsch, J., Weigand, B., Vogiatzaki, K., 2021. Droplet size distributions in cryogenic flash atomization. Int. J. Multiphase Flow 142, 103705.
Lü, M., Ning, Z., Yan, K., Fu, J., Sun, C., 2015. Instability and breakup of cavitation bubbles within diesel drops. Chinese J. Chem. Eng. 23, 262–267.
Luo, M., Haidn, O.J., 2016. Characterization of flashing phenomena with cryogenic fluid under vacuum conditions. J. Propuls. Power 32, 1253–1263.
Lv, M., Ning, Z., Yan, K., 2012. The instability of vapor bubble growth within the diesel droplet under the condition of supercavitation. Adv. Mater. Res. 512-515, 477–480.
Mansour, A., Müller, N., 2019. A review of flash evaporation phenomena and resulting shock waves. Exp. Therm. Fluid Sci. 107, 146–168.
Moulai, M., Grover, R., Parrish, S., Schmidt, D., 2015. Internal and near-nozzle flow in a multi-hole gasoline injector under flashing and non-flashing conditions, SAE Technical Paper Series.
Polanco, G., Holdo, A.E., Munday, G., 2010. General review of flashing jet studies. J. Hazard. Mater. 173, 2–18.
Rees, A., Salzmann, H., Sender, J., Oschwald, M., 2020. About the morphology of flash boiling liquid nitrogen sprays. At. Sprays 30.
Sher, E., Bar-Kohany, T., Rashkovan, A., 2008. Flash-boiling atomization. Prog. Energy Combust. Sci. 34, 417–439.
Soo Yu, Y., Shin, D., Jeong, M., Park, J., Park, S., 2023. Effect on flash boiling spray characteristics in the far-field and near-field and nozzle tip wetting with multi-hole LPDI injector. Appl. Therm. Eng. 219, 119676.
Tang, H., Pan, X., Mei, Y., Wang, X., Zhu, X., Jiang, J., 2022. Morphological characteristics and flashing mechanism of superheated liquid jets released from rectangular breaches. J. Loss Prev. Process Ind. 79, 104840.
Wang, J., Zhou, Z., Chen, B., Yang, T., Zhang, L., Romeos, A., Giannadakis, A., Panidis, T., 2023a. Flow visualization of the transient effect of the internal two-phase flow on the external iso-pentane flashing spray under different injection pressure. Fuel 333, 126151.
Wang, X.-S., Chen, B., Wang, R., Xin, H., Zhou, Z.-F., 2017. Experimental study on the relation between internal flow and flashing spray characteristics of R134a using straight tube nozzles. Int. J. Heat Mass Transf. 115, 524–536.
Wang, Y., Gao, T., Zhou, L., Gong, J., Li, J., 2023b. A parametric study of a hybrid battery thermal management system that couples PCM with wavy microchannel cold plate. Appl. Therm. Eng. 219, 119625.
Wang, Z., Wang, B., Jiang, C., Xu, H., Badawy, T., 2016. Microscopic characterization of isooctane spray in the near field under flash boiling condition. Appl. Energy 180, 598–606.
Witlox, H., Harper, M., Bowen, P., Cleary, V., 2007. Flashing liquid jets and two-phase droplet dispersion II. Comparison and validation of droplet size and rainout formulations. J. Hazard. Mater. 142, 797–809.
Witlox, H.W.M., Fernandez, M., Harper, M., Stene, J., 2017a. Modelling and validation of atmospheric expansion and near-field dispersion for pressurised vapour or two-phase releases. J. Loss Prev. Process Ind. 48, 331–344.
Witlox, H.W.M., Harper, M., Oke, A., Bowen, P.J., Kay, P., 2010. Sub-cooled and flashing liquid jets and droplet dispersion I. Overview and model implementation/validation. J. Loss Prev. Process Ind. 23, 831–842.

Witlox, H.W.M., Harper, M., Webber, D., 2017b. Modeling and validation of dispersion following an instantaneous vapor or two-phase release from a pressurized vessel. Process Saf. Prog. 36, 307–313.
Wu, F., Yu, H., Pan, X., Zang, X., Hua, M., Wang, H., Jiang, J., 2022. Experimental study of methanol atomization and spray explosion characteristic under negative pressure. Process Saf. Environ. Prot. 161, 162–174.
Wu, H., Zhang, F., Zhang, Z., 2021. Fundamental spray characteristics of air-assisted injection system using aviation kerosene. Fuel 286, 119420.
Yildiz, D., Theunissen, R., Beeck, J., Riethmuller, M.L., 2002. Understanding of dynamics of a two-phase flashing jet using multi-intensity-layer PIV and PDA. In: 11th International Symposium on Application of Laser Techniques to Fluid Mechanics. July.
Yildiz, D., vanBeeck, J.P.A.J., Riethmuller, M.L., 2004. Feasibility exploration of laser-based techniques for characterization of a flashing jet. Part. Part. Syst. Charact. 21, 390–402.
Zalkind, V.I., Nizovskiy, V.L., Nizovskiy, L.V., Schigel, S.S., 2021. Features of metastable superheated water atomization when being discharged through convergent-divergent nozzles at different superheat values. J. Phys.: Conference Series 2088, 012054.
Zalkind, V.I., Zeigarnik, Y.A., Nizovskiy, V.L., Nizovskiy, L.V., Schigel, S.S., 2019. Some peculiarities of superheated water flow in contracting-expanding nozzles and their influence on droplet dimension distribution in an atomized water plume. J. Phys.: Conf. Series 1359, 012034.
Zeng, W., Xu, M., Zhang, G., Zhang, Y., Cleary, D.J., 2012. Atomization and vaporization for flash-boiling multi-hole sprays with alcohol fuels. Fuel 95, 287–297.
Zhang, Y., Li, S., Zheng, B., Wu, J., Xu, B., 2015. Quantitative observation on breakup of superheated liquid jet using transparent slit nozzle. Exp. Therm. Fluid Sci. 63, 84–90.
Zhifu, Z., Weitao, W., Bin, C., Guoxiang, W., Liejin, G., 2012. An experimental study on the spray and thermal characteristics of R134a two-phase flashing spray. Int. J. Heat Mass Transf. 55, 4460–4468.
Zhou, Z.-F., Chen, B., Wang, R., Wang, G.-X., 2017. Comparative investigation on the spray characteristics and heat transfer dynamics of pulsed spray cooling with volatile cryogens. Exp. Therm. Fluid Sci. 82, 189–197.
Zhou, Z.-F., Yin, J., Chen, B., Liu, B., Thrassos, P., 2021a. Liquid phase model and its coupling interaction with the ambient gas for the droplet heating and evaporation of highly volatile R134a. Int. J. Heat Mass Transf. 166, 120740.
Zhou, Z.-F., Yin, J., Yang, X.-Y., Chen, B., Liu, B., 2021b. Experimental investigation on the macroscopic spray and microscopic droplet diameter, velocity and temperature of R404A flashing spray. Int. J. Heat Mass Transf. 177, 121546.
Zhu, X., Pan, X., Mei, Y., Ma, J., Tang, H., Zhu, Y., Liu, L.X., Jiang, J., Chen, T., 2023a. Thermal nonequilibrium and mechanical forces induced breakup and droplet formation of superheated liquid jets under depressurized release. Appl. Therm. Eng. 221, 119826.
Zhu, X., Pan, X., Tang, H., Wang, X., Zhu, Y., Liu, L.X., Jiang, J., Chen, T., 2023b. Breakup regime of flashing jet under thermal nonequilibrium and mechanical forces and its relationship with jet characteristics during depressurized releases of superheated liquid. Process Saf. Environ. Prot. 170, 757–770.
Zhu, X., Song, Z., Pan, X., Mei, Y., Wang, X., Zhu, Y., Jiang, J., 2020. Morphological characteristics of flashing jet throughout superheated liquid release. J. Loss Prev. Process Ind. 66, 104163.
Zhu, X., Song, Z., Pan, X., Wang, X., Jiang, J., 2019. Pressure-decay and thermodynamic characteristics of subcooled liquid in the tank and their interaction with flashing jets. J. Hazard. Mater. 378, 120578.